Active Structural Acoustic Control of

Ribbed Plates using a Weighted Sum of Spatial Gradients.

William R. Johnson, Daniel R. Hendricks, and Jonathan D. Blotter

Department of Mechanical Engineering,

Brigham Young University,

Provo,

Utah

84602

Scott D. Sommerfeldt, and Kent L. Gee

Department of Physics and Astronomy,

Brigham Young University,

Provo,

Utah

84602

Abstract

A weighted sum of spatial gradients (WSSG) control metric for use in active structural acoustic control of finite ribbed plates was developed and compared to volume velocity. A finite element model was used to obtain the displacement field on the plate, and a finite difference derivative approach to obtaining the terms in WSSG was used. Previous results of ASAC on finite ribbed plates are minimal in the literature, however volume velocity has been heavily used as a control metric on flat plates. WSSG was compared to volume velocity as a benchmark to measure success of control on a variety of boundary conditions including clamped and simply-supported plates. Simulation results showed that WSSG provided comparable or improved control of radiated sound power on finite ribbed plates on four different boundary conditions. Results also showed that WSSG was relatively insensitive to sensor location, and that multiple control forces could be used to successfully improve control. These results confirm that ASAC can be successfully performed on finite ribbed plates with the WSSG control metric.

I. INTRODUCTION

Active structural acoustic control (ASAC) was first proposed as a method for controlling the sound radiation of distributed structures such as plates and shells[1]. ASAC provided a distinct advantage over active noise control applications to distributed structures by requiring fewer control actuators[2] and removing control actuators from the sound field[3]. Although this method was initially developed with the end goal of minimizing sound radiation from the inside of an airplane fuselage the majority of the literature on ASAC has focused on simple ideal cases such as simply-supported flat plates, while more practical cases, such as ribbed plates (for ship hulls) and cylinders (for modeling aircraft fuselages) have been largely ignored.

Research on flat plates has successfully demonstrated the effectiveness on ASAC, and a variety of methods have been developed for improving ASAC control. Initially ASAC was accomplished by moving the control actuator to the surface of the vibrating structure[4] but it was quickly determined that the error sensor could also be removed from the sound field and placed on the structure as well. This could be done successfully by measuring a quantity on the structure correlated with the radiated sound in the sound field. Control metrics found to be related to this have included squared velocity at a point[5] and volume velocity[6]. One of the early developments and important tools in choosing effective control metrics is the acoustic or radiation mode shapes of a structure[7, 8], which reveal the underlying radiation mechanisms of a structure. The result of the radiation mode shape analysis was the predominance of volume velocity in the literature as a control metric due to its similarity to the first radiation mode.

Volume velocity was shown to provide effective control at many of the natural frequencies of a vibrating plate[6, 7, 9] however it has proved difficult to measure experimentally. A variety of measurement methods have been developed such as accelerometer arrays[9] and distributed piezoelectric films[10]. Shaped PVDF sensors have also been used to target the structural modes associated with specific radiation modes[11, 12] allowing for an alternative to volume velocity in the estimation of the first radiation mode as well as a method to target higher modes. These methods have been effective in measuring volume velocity but their practicality has been hampered by their difficulty of implementation. Accelerometer arrays require too many sensors, distributed PVDF sensors are geometry dependent, and shaped PVDF sensors are mode shape dependent. Thus these methods require *a priori* knowledge of the system, manufacturing processes tailored to the specific geometry, or a complicated experimental setup.

A more recently developed structural metric, termed composite velocity, has been shown to avoid many of these problems[13]. This structural metric was designed to target the first four radiation modes of a plate, was shown to be uniform on a simply supported plate thus making it insensitive to sensor location, and can be measured with an array of four accelerometers without *a priori* knowledge of the structural geometry or modes. This makes it simpler to implement in practice and still provides similar control to volume velocity at structural modes contributing to the first radiation mode, while outperforming it at higher frequencies and structural modes which provide a more significant contribution to the higher radiation modes.

One of the purposes of the current research is to extend the application of the weighted sum and squared gradients (WSSG) metric and the applicability of ASAC on ribbed plates. Until recently

there has not been much theoretical development on ribbed plate vibration. Current research is motivated mainly with reducing ship vibration. Recently models have been developed to represent, analytically, the displacement of a vibrating plate[14, 15, 16] however these require a large number of assumptions to work properly. To mitigate vibration of these plates analysis has shown that ribbed plate vibration can be reduced by irregularly spacing the stiffeners[15, 17]. ASAC has been investigated for an infinite ribbed plate using both line forces[18] and point forces[19] minimizing the far-field acoustic intensity and total sound pressure, respectively. Both of these studies found that significant control could be achieved, however the literature is lacking in exploration of ASAC on finite ribbed plates.

In the literature the concept of ASAC has been demonstrated for flat rectangular plates both numerically and experimentally and shown to work effectively. ASAC has also been simulated for the simplest and most ideal cases of a ribbed plate. The main purpose of this research is to extend the applicability of ASAC on ribbed plates by demonstrating that flat plate objective functions, specifically composite velocity, can be effectively used and applied to achieve control on finite ribbed plates.

II. FORMULATION

For the case of the ribbed plate several different sets of boundary conditions were examined. These were simply-supported plate simply-supported ribs, simply-supported plate free ribs, clamped-plate clamped ribs, and clamped-plate free ribs. Because of the wide variety of boundary conditions examined, and the unavailability of analytical solutions for ribbed plates under these boundary conditions finite element models were used to obtain the displacement of the ribbed plates. For post-processing of the finite element data it is assumed that the ribs do not radiate sound, allowing for the use of the displacement field only on the plate and not on the ribs.

Analytically WSSG is defined as

$$V_{comp}^2 = \alpha \left(\frac{\partial w}{\partial t}\right)^2 + \beta \left(\frac{\partial^2 w}{\partial x \partial t}\right)^2 + \gamma \left(\frac{\partial^2 w}{\partial y \partial t}\right)^2 + \delta \left(\frac{\partial^3 w}{\partial x \partial y \partial t}\right)^2, \tag{1}$$

where w is the displacement of the plate and $\alpha,\ \beta, \gamma$, and δ are the weights for each of the spatial gradients. For this paper all excitations are assumed to be time harmonic which causes each term to be scaled by a constant $j\omega$ which has no effect on the gradient based control algorithm used. Therefore, the time derivative can be removed.

Because of the dependence on finite element data the derivatives can't be taken analytically. Estimates of the terms using finite difference derivatives are defined in Eqs. (2) where the spacing for the finite difference derivatives is shown in Fig. 1. Each of the sensors w_i in Fig. 1 corresponds to the displacement at a nodal location in the finite element data.

$$w \approx \frac{w_1 + w_2 + w_3 + w_4}{4} \tag{2a}$$

$$\frac{\partial w}{\partial x} \approx \frac{w_2 - w_1 + w_4 - w_3}{2\Delta x} \tag{2b}$$

$$\frac{\partial w}{\partial y} \approx \frac{w_1 - w_3 + w_2 - w_4}{2\Delta y} \tag{2c}$$

$$\frac{\partial^2 w}{\partial x \partial y} \approx \frac{w_2 - w_1 + w_3 - w_4}{\Delta x \Delta y} \tag{2d}$$

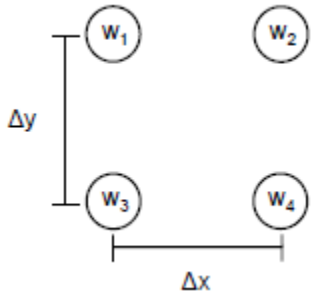

FIG. 1. Geometric configuration of sensors for finite difference derivatives

When WSSG was originally formulated[13] each of the terms was chosen because of their similarity in shape to one of the four most efficiently radiating radiation mode shapes at low frequencies. Although important to the structure and stiffness of the plate, the ribs can be thought of as a line force applied to a flat plate. Thus the radiation mode shapes for the rectangular plate in previous developments still applies to the ribbed plate, suggesting that WSSG has the potential to provide effective control on the ribbed plate.

Also in previous work great care was taken to choose weights which would make the WSSG quantity relatively uniform over the surface of the plate. With the analytical model for the simply-supported flat plate expressions for these weights were derived which scaled each of the terms so that they had the same maximum amplitudes. This resulted in a relatively uniform field which reduced the sensitivity of the WSSG sensor to location. In the case of the ribbed plate, without analytical equations to describe the vibration of the plate analytical weight expressions can't be derived. However the general concept still applies. The weights can be found by calculating each of the WSSG terms over the entire plate for a given frequency and then choosing values for α, β, γ, and δ so that when each term is multiplied by its corresponding weight all of the maximum amplitudes match. This method for choosing weights has been applied throughout this paper for the ribbed plate.

A. The Finite Element Model as a Transfer Function

By assuming that the ribbed plate acts as a linear system the total displacement due to multiple point forces on the plate at a given frequency is the sum of the displacements from the point forces applied individually. Transfer functions from the force location to the sensor location as a function of frequency were created from this data using the standard definition of a transfer function as output over input. For this application the output was displacement at the sensor locations and the input was the applied force.

The displacement at the individual sensor locations (as shown in Fig. 1) in terms of the transfer functions are given in Eqs. (3)

$$w_1 = h_{d_1} F_d + \sum_i h_{ci_1} F_{ci} \tag{3a}$$

$$w_2 = h_{d_2} F_d + \sum_i h_{ci_2} F_{ci} \tag{3b}$$

$$w_3 = h_{d_3} F_d + \sum_i h_{ci_3} F_{ci} \tag{3c}$$

$$w_2 = h_{d_3} F_d + \sum_i h_{ci_3} F_{ci} \tag{3d}$$

where h_d are the transfer functions from the applied disturbance to the first, second, third, or fourth sensor in the array, and h_{ci} are the transfer functions from the ith applied control force to the first, second, third, or fourth sensor in the array and F_d and F_{ci} are the corresponding disturbance and control forces. Substituting these expressions into Eqs (2) allows for the calculation of WSSG. After this substitution the individual transfer functions can be rearranged to create more general transfer functions in terms of the derivatives. This is shown in Eqs. 4 with F_d assumed to have a value of unity

$$w \approx \frac{h_{wd} + \sum_i h_{wc_i} F_{c_i}}{4} \tag{4a}$$

$$\frac{\partial w}{\partial x} \approx \frac{h_{\frac{\partial w}{\partial x} d} + \sum_i h_{\frac{\partial w}{\partial x} c_i} F_{c_i}}{2\Delta x} \tag{4b}$$

$$\frac{\partial w}{\partial y} \approx \frac{h_{\frac{\partial w}{\partial y} d} + \sum_i h_{\frac{\partial w}{\partial y} c_i} F_{c_i}}{2\Delta y} \tag{4c}$$

$$\frac{\partial^2 w}{\partial x \partial y} \approx \frac{h_{\frac{\partial^2 w}{\partial x \partial y} d} + \sum_i h_{\frac{\partial^2 w}{\partial x \partial y} c_i} F_{c_i}}{\Delta \mathrm{x} \Delta y} \tag{4d}$$

where h_w, $h_{\frac{\partial w}{\partial x}}$, $h_{\frac{\partial w}{\partial y}}$, and $h_{\frac{\partial^2 w}{\partial x \partial y}}$ are the transfer functions for the derivative terms, and can be expressed as

$$h_w = h_1 + h_2 + h_3 + h_4 \tag{5a}$$

$$h_{\frac{\partial w}{\partial x}} = h_2 - h_1 + h_4 - h_3 \tag{5b}$$

$$h_{\frac{\partial w}{\partial y}} = h_1 - h_3 + h_2 - h_4 \tag{5c}$$

$$h_{\frac{\partial^2 w}{\partial x \partial y}} = h_2 - h_1 + h_3 - h_4 \tag{5d}$$

Using WSSG in this form allows for the calculation of displacements using the finite element data and the optimization of the control force external to the finite element code. The radiated sound power could then be calculated by calculating the average velocity of each element due to the disturbance and optimized control forces and then using the radiation resistance matrix method[7].

This method was validated by simulating control of WSSG on a simply-supported flat (no ribs) plate using both analytical and FEA formulations using the same dimensions and material properties as previous work[13] on WSSG for a simply-supported plate. This simulation can be seen in Fig. 2. Note in the simulation that both the radiated power before control and after control match up very closely in the analytical and finite element cases. The slight discrepancies seen can be attributed to the discretization and numerical error of the finite element model, as well as the difference in taking finite difference derivatives as opposed to the exact derivatives of the analytical model. The overall match between the two models demonstrates that the method described above using the finite element data is an accurate approximation and can be used to effectively predict the radiated sound power and find optimal control forces to minimize it.

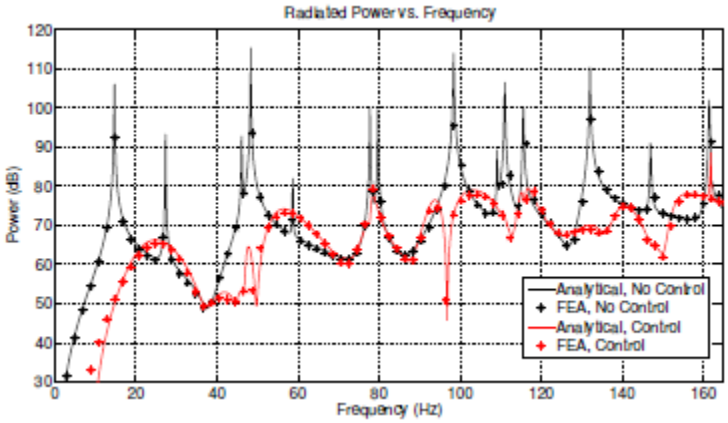

FIG. 2. Simulated control for a flat simply-supported plate using both analytical and finite element models

III. SIMULATIONS

To demonstrate the effectiveness of WSSG as a control metric, simulations on a ribbed plate are presented in this section. Several specific cases were of interest because of the manner in which WSSG was developed. First, control of WSSG on a variety of boundary conditions is shown to demonstrate its applicability to a wide variety of situations. Second, simulations to demonstrate the insensitivity of the control provided by WSSG to the measurement point are shown to demonstrate the effectiveness of the uniformity of the control field. Last of all, control of the ribbed plate with multiple applied control forces is demonstrated to show how control can be achieved over a larger range of natural frequencies.

The typical geometry and distances for the simulation are shown in Fig. 3 where the subscript d stands for disturbance, s stands for sensor, c stands for control, and L_x and L_y are the lengths in x and y respectively. A finite element model defined by this geometry was created. Geometric

and material properties for the model are shown in Table I. The model used has two ribs placed at $x = 1/3L_x, 2/3L_x$ dividing the plate into left, middle, and right sections.

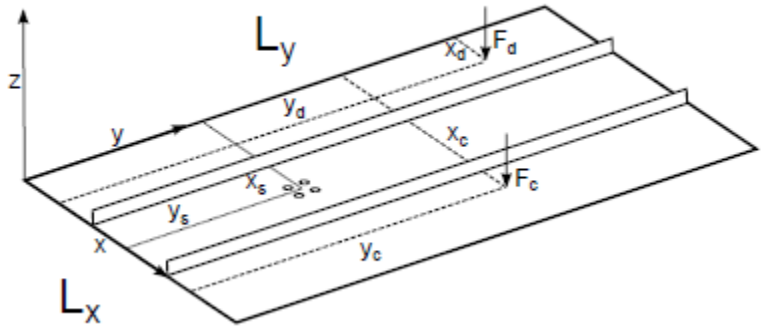

FIG. 3. Typical geometry of the ribbed plate

Using finite element software the displacement of the plate due to an individual unit point force at chosen disturbance and control locations was found. The point forces were applied harmonically over the frequency range from 0 Hz up to the fifteenth structural mode natural frequency (ranging from 220 - 280 Hz depending on the boundary conditions).

A. Effectiveness of WSSG on Different Boundary Conditions

Using the formulation described previously ASAC on the ribbed plate shown in Fig. 3 with the properties given in Table I was simulated under the four boundary conditions: simply-supported plate, simply supported ribs; simply-supported plate, free ribs; clamped plate, clamped ribs; and clamped plate, free ribs with the disturbance, control and sensor locations given in Table II. Note that for this case both the disturbance and control reside in the left-most section of the ribbed plate, and the sensor lies in the center section. In each of the simulations WSSG was compared with volume velocity, the most commonly used ASAC metric, for the ribbed plate.

Fig. 4 shows control of the simply-supported plate simply-supported ribs boundary condition. On this boundary condition, over the frequency range shown in the figure, WSSG has an average attenuation of 4.8 dB compared to an average attenuation of 5.1 dB for volume velocity, thus both control metrics provide comparable control for the plate; however there are several differences. WSSG controls modes 3, 8, 9, 10, and 14 while volume velocity doesn't. Volume velocity controls modes 2, 4, 7, and 13 much better than WSSG. Neither can control modes 5 and 6, which are close enough together to be considered a degenerate mode. Also, mode 15 which is at about 235 Hz has no noticeable sound radiation. This is due to the ribs constraining the plate to an extremely small displacement at this mode.

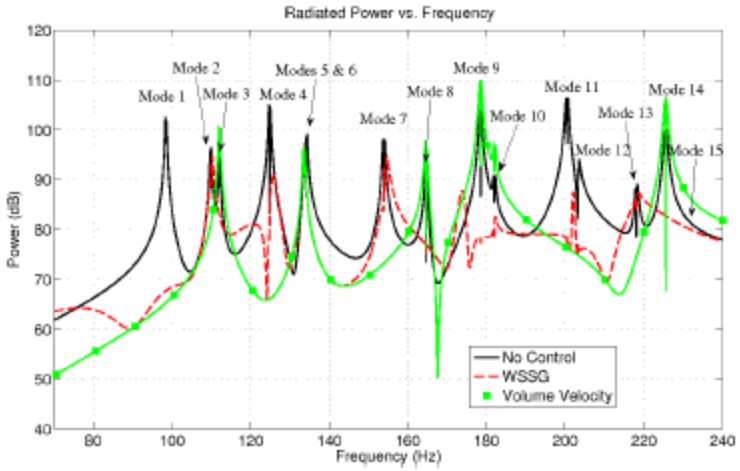

FIG 4. Simulated control of the ribbed plate with the simply-supported plate simply-supported ribs boundary condition

Fig. 5 shows control of the simply-supported plate free ribs boundary condition. The average attenuation for both WSSG and volume velocity, respectively, was 6.9 dB and 5.6 dB, so in this case WSSG outperforms volume velocity over the frequency range shown by about 1.3 dB. In particular note that WSSG achieves control at modes 4, 8, 9, 11, and 15 while volume velocity outperforms WSSG only at modes 7 and 14.

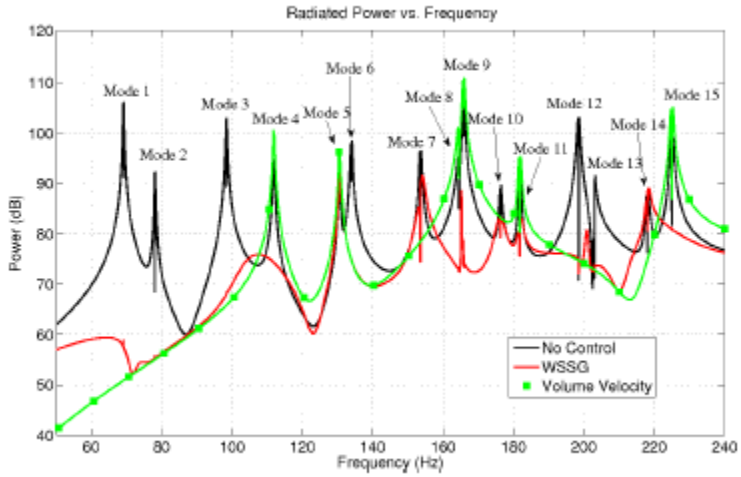

FIG. 5. Simulated control of the ribbed plate with the simply-supported plate free ribs boundary condition

For the clamped plate clamped ribs boundary conditions simulated control can be seen in Fig. 6. For the clamped plate the average attenuation for WSSG over the frequency range shown is 3.4 dB while for volume velocity the average attenuation is 4.3 dB, a 0.9 dB difference. In this case the difference in control is due to the success of volume velocity at the degenerate modes 3 and 4. In particular in mode 4 there is no intercellular cancellation, resulting in a large net volume

velocity, thus allowing volume velocity to be an effective metric for this mode. Beyond modes 3 and 4 WSSG performs on par with or better than volume velocity at each of the modes. One mode of particular note is the mode at approximately 235 Hz which is a triply degenerate mode, causing difficulty for both control metrics.

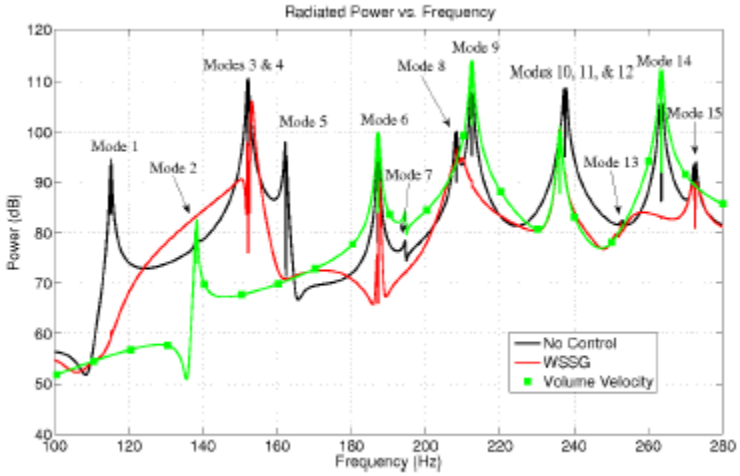

FIG. 6. Simulated control of the ribbed plate with the clamped plate clamped ribs boundary condition

The clamped plate free ribs boundary condition simulated control is shown in Fig. 7. Under this boundary condition the WSSG control metric provides an average attenuation of 6.4 dB over the frequency range shown, while volume velocity provides an average attenuation of 5.4 dB, thus WSSG outperforms volume velocity in this case as well. For control on this boundary condition note in particular the control of modes 6, 8, and 14, where WSSG provides improved control over volume velocity. Also, for this boundary condition a triply degenerate mode occurs around 235 Hz which neither metric can control.

From the previous simulation results it can be concluded that the ribbed plate can be controlled by both volume velocity and WSSG, and that they provide comparable control. Two questions of interest at this point include why sound radiation control is achieved at some structural modes and not others, and what effects the ribs have on the ability of the control metrics to provide control of sound radiation. The shapes of the structural modes provide some insight into these two questions.

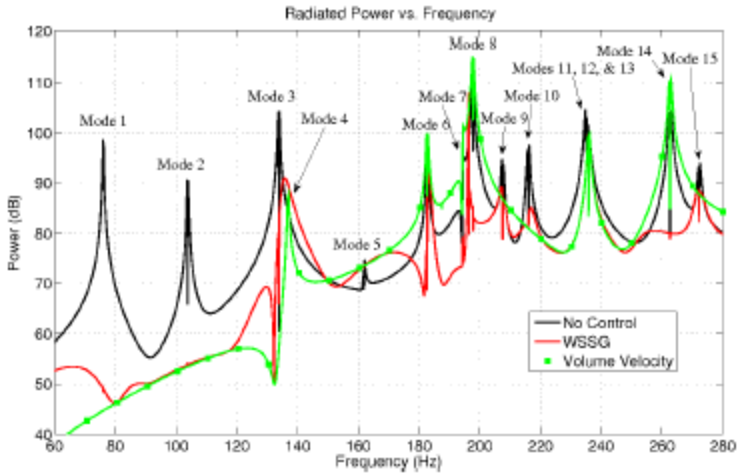

FIG. 7. Simulated control of the ribbed plate with the clamped plate free ribs boundary condition

With the plate divided into three sections by the ribs the lower structural modes are constrained so that their nodal lines fall on the locations of the ribs. This causes the ribbed plate to look like three separate vibrating plates. On flat plates WSSG was found to be relatively uniform over the entire plate with the correct weights chosen. This is not the case for the ribbed plate. Instead, the ribbed plate tends to be uniform within each section of the plate, but not necessarily uniform for the entire plate. In particular at some natural frequencies the middle section of the plate, between the two ribs, has extremely small amplitude vibration when compared to the outer two sections.

For example, in Fig. 8 the WSSG field of the simply-supported plate free ribs mode 5 is shown. On this mode there is very little displacement in the middle section, the majority of the motion occurs between the ribs and the plate edges. For the simulations the sensor was placed in the middle section, measuring very small values for WSSG and therefore was unable to provide control to the sections of the plate which were radiating. This was the case on the majority of the modes where WSSG was unsuccessful, irrespective of boundary conditions.

B. WSSG Sensitivity to Sensor Location

For flat plate cases because WSSG was relatively uniform the control was shown to be relatively independent of sensor location. This claim can't quite be made on the ribbed plate due to the large difference in the WSSG values between sections of the plate at some frequencies. However, each individual section is relatively uniform, therefore independence of sensor location would be expected within a given section of the plate. In order to investigate this effect the disturbance and control forces were held constant at their previous locations in the left section of the plate, and control was simulated with the sensor placed at four different sensor locations within each of the three sections of the plate.

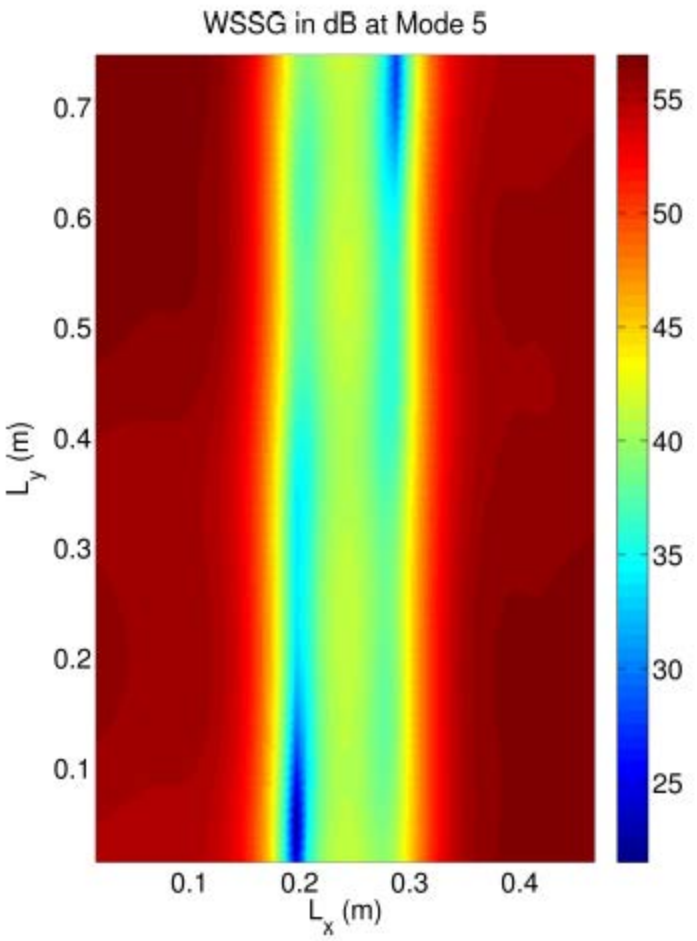

FIG. 8. The simply-supported plate simply supported boundary condition mode 2 WSSG field for the ribbed plate

Fig. 9 shows the simulated control at the different sensor locations spread across the left section. For this case the control is very similar across the entire frequency range, particularly above the second mode. At many frequencies the similarity in control is so close that all of the control models overlap. Also note that the fifth mode where control could not be achieved previously (see Fig. 5) is now being controlled. This is because the left section has large motion at this mode, as shown in Fig. 8.

Control for the middle section of the plate at the different sensor locations is shown in Fig. 10. Note again the similarity of control between the four different sensor locations. For this case specifically note the fifth mode again, where none of the sensors can achieve control. This is because of the extremely low amplitude of the WSSG field, as shown in Fig. 8. At this mode because the value of WSSG is already so close to zero at the sensor location the control force is unable to provide any meaningful control for motion of the plate elsewhere.

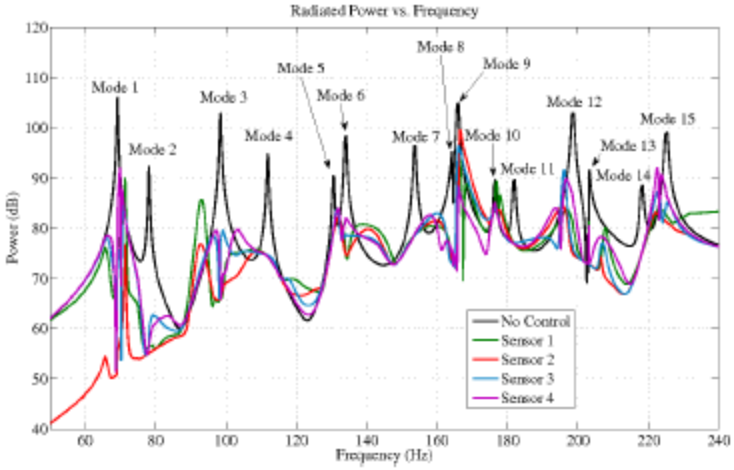

FIG. 9. Simulated control at various sinsor locations in the left section

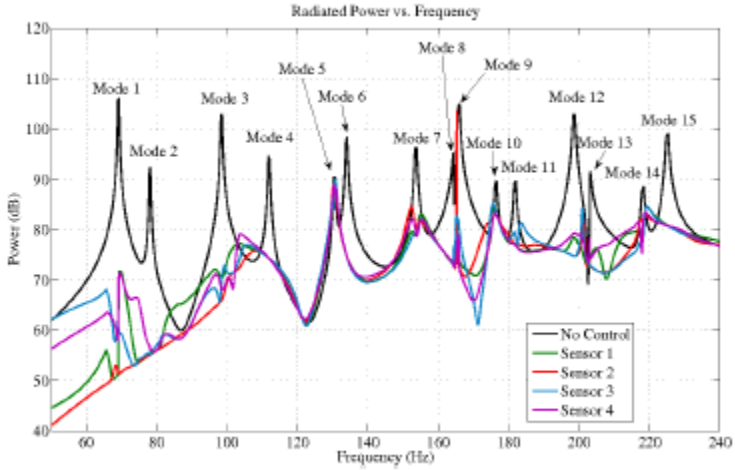

FIG. 10. Simulated control at various sensor locations in the middle section

Finally, the right bin simulated control for the separate sensor locations is shown in Fig. 11. Once again the control for each individual sensor is very similar to all the others, although not exact. Note that control is once again achieved at the fifth mode, due to the large magnitude of the WSSG field, as shown in Fig. 8. Also of importance is that the disturbance and control forces were kept in their usual locations, in the leftmost section. Control is not quite as consistent, particularly near modes 8 and 9 because of the relatively long distance between the sensors and location of the control force application. At this sensor location the vibrations created by the control force are impeded by both ribs, thus affecting control.

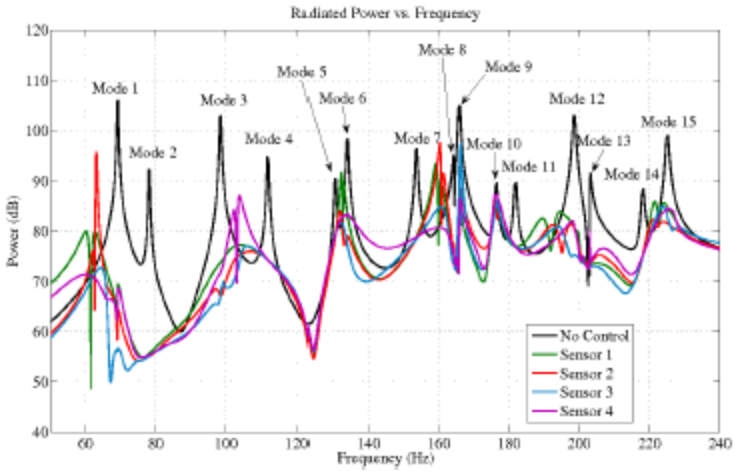

FIG. 11. Simulated control at various sensor locations in the right section

From the above simulations and analysis it can be concluded that the WSSG control metric is largely independent of sensor location within each section of the plate, but that it varies from section to section because of the way in which the mode shapes are modified by the ribs as well as the barrier which the ribs provide to wave propagation from the control force. Thus if each individual section were considered a separate plate these results are consistent with the simulated results for WSSG on a flat rectangular plate.

C. Multi-force Control

The last case of interest in examining the ability of WSSG to control the vibrating plate is applying multiple control forces in an effort to minimize the radiated sound power. It was expected that by applying multiple control forces control could be improved at modes where poor control was originally achieved.

For the investigation of this problem the disturbance and first control forces were kept at the same places as previously, in the left section of the plate, and the sensor was also kept at the same location in the middle of the plate. The second control force was applied in the right section of the plate, and an optimization algorithm was used to determine the control force values which minimized the WSSG quantity at the measurement location. A figure showing the two control forces controlling the radiated sound power separately is shown in Fig. 12.

One of the important differences between the two control models is that the original control location is unable to control the fifth mode as stated previously but the alternate control location does obtain control. Also of note is the ninth mode, which neither force controls well, and the twelfth mode, which the original controls well, but the alternate doesn't.

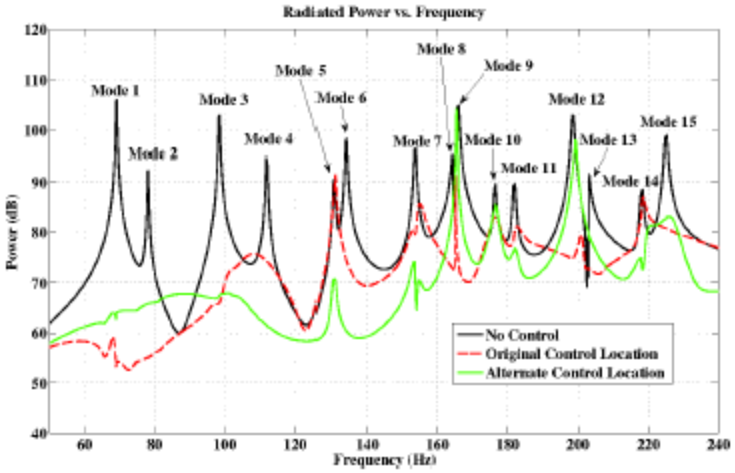

FIG. 12. Simulated control of the plate with the two control forces applied separately

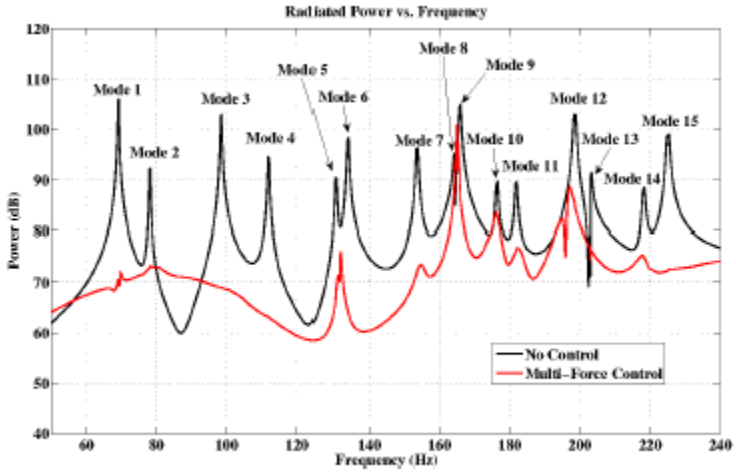

FIG. 13. Simulated control of the plate with the two separate control forces applied simultaneously

The simulated control with both forces minimizing WSSG together is shown in Fig. 13. Control of WSSG with both forces controlling simultaneously appears similar in some aspects to control with each of the forces applied separately. There are several points of particular importance in this figure. At the 5th mode the two combined control forces can achieve control, this is due to the effectiveness of the alternate control force here. A similar situation appears at mode 12, but the roles are reversed. At the 9th mode, because neither force could provide good control individually no control is achieved when they are applied simultaneously.

One other point of importance is the off-resonance control at about 85 Hz. Notice that the radiated sound power is actually amplified here, worse than either model previously. In general poor control can be observed at off-resonance frequency values in all of the previous results. For

example in Figs. 2, 4, and 5 control is generally not achieved off-resonance with either WSSG or volume velocity.

Fig. 14 shows the minimized WSSG values on a semi-log scale for each of the control forces separately and applied simultaneously. At or near natural frequencies it can be seen that minimizing WSSG does correlate with reducing the radiated sound power. For example at mode 5 the original control force was unable to minimize WSSG therefore control was not achieved, but the alternate force did minimize WSSG, therefore mode 5 was controlled with regards to radiated sound power. However at off-resonances, for example 85 Hz, it can be seen that this is not necessarily the case. The values of WSSG were minimized by all three control cases but none of them provided control.

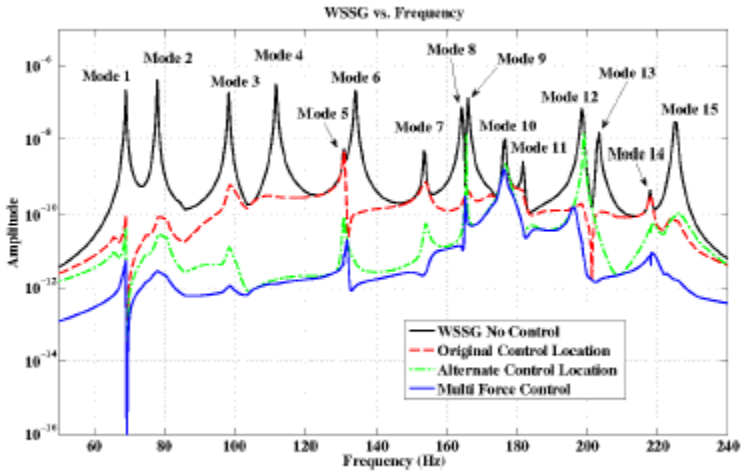

FIG. 14. Minimized WSSG quantities on the simply-supported plate free ribs boundary condition.

In general across the entire frequency spectrum the minimized value of the multi-force control can be seen to be less than or equal to the minimized value of the two models applied individually, verifying that improved control of WSSG is achieved with multiple control models. However, in light of the radiated sound power plots it can be concluded that improved control of WSSG at off-resonances doesn't necessarily correlate to better control of radiated sound power at off-resonances. This unexpected result calls into question how well the derivative terms in WSSG (as shown in Eq. (2)) actually correlate to the radiation mode shapes as has been claimed previously[13]. Also, because of its poor control at off-resonance frequencies and development in targeting the first radiation mode shape[7] volume velocity would also fall prey to this problem.

From the preceding analysis it can be inferred that to achieve control at natural frequencies complementary control force locations should be chosen so as to cover the widest range of possible natural frequencies. However, this method is unlikely to improve control of radiated sound power at off-resonance frequencies due to the lack of correlation between WSSG and radiated sound power.

IV. Conclusions

The WSSG control approach was tested, through simulations, for effectiveness in reducing the radiated sound power of ribbed vibrating plates. In the first set of simulations control of the ribbed plate under four boundary conditions: simply-supported plate, simply-supported ribs; simply-supported plate, free ribs; clamped plate, clamped ribs; and clamped plate, free ribs, was shown. This set of simulations showed that control of radiated sound power on all of these plates could be achieved by using WSSG as a control metric. The control of WSSG was compared to volume velocity, the most common control metric in the literature, and was found to provide similar or improved control in all four boundary condition cases. Through this set of simulations it can be concluded that WSSG is applicable to a wide variety of boundary conditions and can successfully provide control.

In the second set of simulations the simply-supported plate free ribs boundary condition was investigated for insensitivity to sensor location, as claimed in the formulation, by simulating control with the WSSG sensor placed in many locations across the plate. Results showed that although control was not consistent across the entire plate due to the mode shapes created by the ribs, control of varying sensor locations in each individual section of the plate created by the ribs was very consistent.

In the third set of simulations a second control force was added in an attempt to improve control, particularly of natural frequencies that were uncontrolled by the individual model. These simulations showed that control of the natural frequencies could be improved by adding another control force, but at the potential cost of amplifying the off-resonance frequencies' radiated sound. This was inferred to be the case due to a lack of correlation between the terms of the WSSG metric and the radiation mode shapes, away from natural frequencies.

To summarize WSSG was found to be an effective control metric for a rectangular ribbed plate. It was shown to provide comparable or better sound control to volume velocity, achieved this control with fewer sensors and independent of geometry, and to work effectively with multiple control forces.

References

[1] C. R. Fuller, "Active control of sound transmission/radiation from elastic plates by vibration inputs: I. analysis", Journal of Sound and Vibration **136**, 1 – 15 (1990).

[2] J. D. Jones and C. R. Fuller, "Active control of sound fields in elastic cylinder by multi control forces", American Institute of Aeronautics and Astornautics Journal **27**, 845 – 852 (1989).

[3] F. Fahy and P. Gardonio, *Sound and Structural Vibration*, 2nd edition (Academic Press, Amsterdam London) (2007).

[4] C. R. Fuller, C. H. Hansen, and S. D. Snyder, "Active control of sound radiation from a vibrating rectangular panel by sound sources and vibration inputs: an experimental comparison", Journal of Sound and Vibration **145**, 195 – 215 (1991).

[5] C.-C. Sung and C. T. Jan, "Active control of structurally radiated sound from plates", Journal of the Acoustical Society of America **102**, 370 – 381 (1997).

[6] M. E. Johnson and S. J. Elliott, "Active control of sound radiation using volume velocity cancellation", Journal of the Acoustical Society of America **98**, 2174 – 2186 (1995).

[7] S. J. Elliott and M. E. Johnson, "Radiation modes and the active control of sound power", Journal of the Acoustical Society of America **94**, 2194 – 2204 (1993).

[8] K. Naghshineh and G. H. Koopmann, "Active control of sound power using acoustic basis functions as surface velocity filters", Journal of the Acoustical Society of America **93**, 2740 – 2752 (1993).

[9] T. C. Sors and S. J. Elliott, "Volume velocity estimation with accelerometer arrays for active structural acoustic control", Journal of Sound and Vibration **258**, 867 – 883 (2002).

[10] P. Gardonio, Y.-S. Lee, and S. J. Elliott, "Analysis and measurement of a matched volume velocity sensor and uniform force actuator for active structural acoustic control", Journal of the Acoustical Society of America **110**, 3025 – 3031 (2001).

[11] S. D. Snyder, N. Tanaka, and Y. Kikushima, "The use of optimally shaped piezo-electric film sensors in the active control of free field structural radiation, Part 1: Feedforward control", Journal of Vibration and Acoustics **117**, 311 – 322 (1995).

[12] S. D. Snyder, N. Tanaka, and Y. Kikushima, "The use of optimally shaped piezo-electric film sensors in the active control of free field structural radiation, part 2: Feedback control", Journal of Vibration and Acoustics **118**, 112–121 (1996).

[13] J. M. Fisher, J. D. Blotter, S. D. Sommerfeldt, and K. L. Gee, "Development of a pseudo-uniform structural quantity for use in active structural acoustic control of simply supported plates: An analytical comparison", Journal of the Acoustical Society of America **131**, 3833 – 3840 (2012).

[14] T. R. Lin and J. Pan, "A closed form solution for the dynamic response of finite ribbed plates", Journal of the Acoustical Society of America **119**, 917–925 (2006).

[15] T. R. Lin, "A study of modal characteristics and the control mechanism of finite periodic and irregular ribbed plates", Journal of the Acoustical Society of America **123**, 729 – 737 (2008).

[16] T. R. Lin, "An analytical and experimental study of the vibration reponse of a clamped ribbed plate", Journal of Sound and Vibration **331**, 902–913 (2012).

[17] T. R. Lin, J. Pan, P. J. O'Shea, and C. K. Mechefske, "A study of vibration and vibration control of ship structures", Marine Structures **22**, 730 – 743 (2009).

[18] Y. Gu and C. R. Fuller, "Active control of sound radiation due to subsonic wave scattering from discontinutities on fluid-loaded plates. i: Far-field pressure", Journal of the Acoustical Society of America **90**, 2020–2026 (1991).

[19] N. J. Kessissoglou and J. Pan, "Active structural acoustic control of an infinite ribbed plate under light fluid loading", Journal of the Acoustical Society of America **104**, 3398–3407 (1998).

TABLE I. Geometric and material properties used in the finite element model

Quantity	Value
L_x	0.483 m
L_y	0.762 m
Plate thickness	0.001 m
Rib height	0.025 m
Rib thickness	0.0009 m
Young's modulus	207 GPa
Poisson's ratio	0.29
Density	7800 kg/m^3

TABLE II. Geometric and material properties used in the finite element model

Quantity	Value
x_d	0.0805 m
y_d	0.635 m
x_c	0.0805 m
y_c	0.127 m
x_s	0.286 m
y_s	0.432 m